Title

Critical Role of Thermal Fluctuations for CO Binding on Electrocatalytic Metal Surfaces

Journal

JACS Au, 1(10)

ISSN

2691-3704

Authors

Li, Wan-Lu

Lininger, Christianna N

Chen, Kaixuan

et al.

Publication Date

2021-10-25

DOI

10.1021/jacsau.1c00300

Peer reviewed

JACS Au
AN OPEN ACCESS JOURNAL OF THE AMERICAN CHEMICAL SOCIETY

pubs.acs.org/jacsau

Article

Critical Role of Thermal Fluctuations for CO Binding on Electrocatalytic Metal Surfaces

Wan-Lu Li, Christianna N. Lininger, Kaixuan Chen, Valerie Vaissier Welborn, Elliot Rossomme, Alexis T. Bell, Martin Head-Gordon, and Teresa Head-Gordon*

Cite This: https://doi.org/10.1021/jacsau.1c00300

Read Online

ACCESS | Metrics & More | Article Recommendations | Supporting Information

ABSTRACT: This work considers the evaluation of density functional theory (DFT) when comparing against experimental observations of CO binding trends on the strong binding Pt(111) and intermediate binding Cu(111) and for weak binding Ag(111) and Au(111) surfaces important in electrocatalysis. By introducing thermal fluctuations using appropriate statistical mechanical NVT and NPT ensembles, we find that the RPBE and B97M-rV DFT functionals yield qualitatively better metal surface strain trends and CO enthalpies of binding for Cu(111) and Pt(111) than found at 0 K, thereby correcting the overbinding by 0.2 to 0.3 eV to yield better agreement with the enthalpies determined from experiment. The importance of dispersion effects are manifest for the weak CO binding Ag(111) and Au(111) surfaces at finite temperatures in which the RPBE functional does not bind CO at all, while the B97M-rV functional shows that the CO−metal interactions are a mixture of chemisorbed and physisorbed species with binding enthalpies that are within ∼0.05 eV of experiment. Across all M(111) surfaces, we show that the B97M-rV functional consistently predicts the correct *atop* site preference for all metals due to thermally induced surface distortions that preferentially favor the undercoordinated site. This study demonstrates the need to fully account for finite temperature fluctuations to make contact with the binding enthalpies from surface science experiments and electrocatalysis applications.

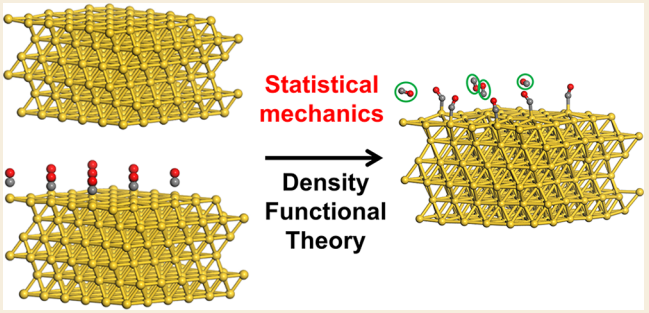

KEYWORDS: *thermal fluctuations, surface relaxation, CO binding, density functional theory*

INTRODUCTION

The electrochemical CO_2 reduction reaction (CO2RR) is one of the most promising technologies available for converting greenhouse gases into useful chemicals using renewable energy sources.[1−3] Given the low concentration of CO_2 adsorbed at the active metal interface, the inherent mechanism of CO2RR has proved to be difficult to investigate experimentally, although new spectroscopic surface sensitive and *operando* measurements are starting to emerge.[4] To address mechanistic questions, density functional theory (DFT) is almost universally used in catalysis modeling today,[5] typically at the level of a generalized gradient approximation (GGA) due to its lower computational cost and reasonable accuracy for molecular chemistry, but has yielded mixed success for modeling surfaces important to heterogeneous catalysis. A particular Achilles heel has been the inability to predict adsorption energies and adsorption-site preferences on electrocatalytically relevant metals; in particular, it has been a challenge for DFT to accurately predict the surface properties and preferred adsorption sites for the CO intermediate of CO2RR on electrocatalytically relevant metals with weak (Ag, Au) and strong (Cu, Pt) binding surfaces.[6,7]

The reasons for these failures are due to many competing effects that make the theoretical approach challenging: the inexact exchange−correlation term of all DFT functionals[8] including lack of nonlocal correlation which is necessary to describe dispersion interactions,[9] accounting of zero point energies,[10] the quality and consistency of the pseudopotentials used,[11] missing *a posteriori* thermodynamic corrections,[12,13] the breakdown of the Born−Oppenheimer approximation and electronic-vibrational coupling,[14−16] and significant variations in binding enthalpies among surface science experiments[17,18] and their thermodynamics interpretations.[19] A compact summary of the current state of affairs offered by Wellendorff and co-workers is that the gas adsorbate−metal binding energies calculated from DFT exhibit an average difference of ∼0.3 eV across experimental systems, showing that there is ample room for further improvements in the theoretical approach.[20]

To illustrate, numerous theoretical studies have reported the drawbacks of the GGA functionals on predicting the physical

Received: July 5, 2021

and chemical properties of gas−solid metal surfaces.[21−24] In response, a number of GGA functionals have been developed to better reproduce adsorption energies, such as the RPBE GGA functional which fulfills the Lieb−Oxford criterion by construction.[21] Another alternative is to investigate other classes of DFT functionals. For example, the random phase approximation (RPA), located at rung five on the Jacob's ladder hierarchy, can overcome some of the failures of semilocal functionals and even some hybrid functionals in various surface science applications.[25−29] Relevant to this study, RPA predicts the preferred *atop* site for CO adsorption on the 0 K surfaces of Pt(111) and Cu(111),[24,30,31] in good to excellent agreement with experimental observations, which emphasizes the importance of nonlocal correlation. Although a number of new hybrid DFT functionals that incorporate exact-exchange and range-separation are available,[32−35] they are not viable given their computational expense and the long-term goal of a complete description of the gas−solid or solid−liquid interfacial chemical reactions.

One rung higher from the GGA on Jacob's ladder are the meta-GGA functionals that incur ∼4 times the expense of a GGA, and thus, these are possible contenders for a complete DFT model for electrocatalysis that includes the liquid due to their affordability. Just recently, a benchmark study including RPBE and the meta-GGA functionals SCAN,[36−38] RTPSS,[39] and B97M-rV[40,41] models reported on their ability to reproduce experimental surface relaxation properties, and CO adsorption energies and site preferences, on the M(111), where M = Pt, Cu, Ag, Au metal, surfaces.[42] While RPBE performed well for the benchmark bulk and surface relaxation properties, the first-principles SCAN[36,37] and semiempirical RTPSS[39] and B97M-rV[40,41] meta-GGA functionals yielded mixed results, displaying under-relaxed surface layer displacements and/or strong overbinding of CO on Pt and Cu. Disappointingly, all lower-rung DFT functionals considered did not predict the CO adsorption site preference for Cu(111) and Pt(111), the *atop* site for all metals observed at low CO adsorbate coverage, instead predicting stronger binding to multicoordinated metal sites.

But as is standard in nearly all surface science computational work, DFT functionals are evaluated at 0 K, while all metal surfaces, adsorbants, and reactions are experimentally produced under finite temperature conditions. In fact Guo et al. showed that free energy can differentiate among CO binding sites for Pt(111) using the PBE functional.[43] Hence the culmination of the literature indicates that there may be an important interplay between the quality of DFT functional with a commensurate pseudopotential and the statistical fluctuations introduced by finite temperature that can change the stability and site preference of the CO bound state.[44] To address the former aspect of surface science modeling, we compare the computationally affordable and popular GGA functional RPBE[42] because it corrects the well-known overbinding problem of PBE for CO on Pt(111) at 0 K[21] as well as the semiempirical meta-GGA functional B97M-rV[40,41] which has also shown promise by correctly describing intermolecular interactions for many molecular systems. To address the statistical mechanics, we have performed unconstrained *ab initio* molecular dynamics (AIMD)[45] in the NVT and NPT ensembles to better compare to experimental conditions for evaluating observables such as bulk and surface relaxation properties, CO adsorption enthalpies, and site preferences and by considering a range of strong to weak CO-binding M(111) surfaces where M = Pt, Cu, Ag, Au. Because most experiments report enthalpies of binding from temperature-programmed desorption (TPD),[18−20,46] single crystal adsorption calorimetry,[20,47,48] and low energy electron diffraction,[49−53] we only consider enthalpies at 300 K in this study, a point to which we return to in the Discussion. We note that the experimental methods provide an accurate activation energy under the assumption that the adsorption ↔ desorption process is reversible and the adsorption barrier is negligible.

Our results show that both the RPBE and B97M-rV functionals exhibit a greater expansion of the top layers of the bare M(111) surface at finite temperature, which in turn considerably addresses the CO overbinding issue when evaluated at 300 K relative to 0 K, by as much as ∼0.3 eV/CO for Pt(111). At the same time, higher quality pseudopotentials and thermalization also expose the importance of dispersion interactions, with only the B97M-rV functional predicting the correct atop site preference for CO binding for Cu(111) and Pt(111) while also describing the weak binding for the Ag(111) and Au(111) metals which can now be seen as arising as a mixture of chemisorbed and physisorbed CO species that quantitatively reproduces the experimental enthalpies. Overall, the accounting of statistical fluctuations of a thermalized ensemble is shown to improve DFT agreement with experimental binding enthalpies across four different metals with a range of CO-binding strengths and shows that DFT functionals with dispersion offer a more balanced performance for the gas−solid interface, setting the stage for future studies involving more realistic and robust theoretical models of surface science and the liquid−solid interface of electrocatalytic devices.

RESULTS

The model for the bulk metal and bare M(111) surfaces and adsorbate−surface sites are provided in Figure 1a. Six metal layers are employed in total to describe the surface layer and bulk character of the metals, with each layer containing 36 (6 × 6) metal atoms and then imposing periodic boundary conditions in the $x-y$ plane; there are no constraints used to fix layers. All *ab initio* molecular dynamics (AIMD) simulations are performed in the NVT ensemble by imposing the known lattice structure of each metal. Surprisingly, the Au(111) and Ag(111) systems using RPBE were found to distort due to its inability to adopt the experimental lattice volume in the NVT ensemble, and we thus performed these RPBE systems in the NPT ensemble (at 1 atm pressure) in order to allow adjustments to stable bulk structures. The B97M-rV functional optimized well to the experimental lattice in the NVT ensemble.

CO adsorption properties are averaged across 9 CO molecules chosen to reproduce a low ∼25% coverage that matches the reported experimental conditions of low coverage by Wellendorf and co-workers (Figure 1b).[20] All AIMD simulations reported are comprised of 2 ps trajectories, with statistics for observables collected over the last 1.5 ps. In this work, we have used the existing pseudopotentials (PP) for PBE for RPBE: a small-core PP for Pt and a large-core PP for the other metals. We have optimized small core pseudopotentials and the corresponding basis sets consistent with the B97M-rV functional when used in CP2K.[54] Further details of the results reported here are provided in the Materials and Methods and in the Supporting Information (SI).

Interlayer Relaxation of Metal Surfaces

It is known that metal surface strain trends directly contribute to a finely balanced occupation of metal *d* states for correct

https://doi.org/10.1021/jacsau.1c00300
JACS Au XXXX, XXX, XXX−XXX

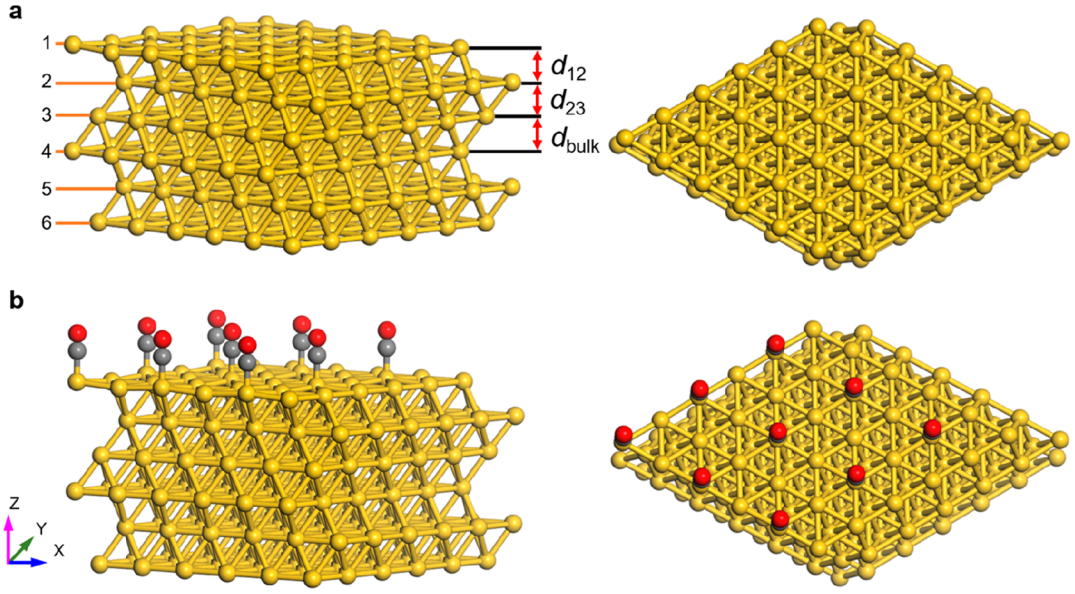

Figure 1. Bulk metal and metal surface models used to describe structural relaxations and CO binding preferences. (a) The 6 × 6 model for the bare M(111) surface, with interlayer distances d_{12} and d_{23}. In the 0 K calculation, the bottom three layers are frozen so that d_{bulk} is the distance defined over the last two interlayer distances. For finite temperature, the d_{bulk} value is defined as the averaged distance between third and fourth layer during MD simulation. We tested the number of frozen layers on supercells from 2 × 2 × 2 to 8 × 8 × 8 models and found the unconstrained 6 × 6 × 6 super cell to be most reliable at finite temperature. (b) Initial condition of nine adsorbed CO molecules on the surface, from two different perspectives corresponding to a low coverage result of 0.25; only the *atop* site configuration is shown here, but a similar set up was used for the initial condition of the other three multicoordinated sites (*bridge*, *fcc*, and *hcp* shown in SI Figure S1) for Pt(111) and Cu(111).

adsorbate−surface interactions.[55] We therefore first test whether thermalization can give rise to better surface strain trends for the DFT functionals investigated here (Figure 2). We first carried out static calculations at 0 K with the RPBE and B97M-rV functionals for the metal models (Figure 1) to determine interlayer distance d_{12}, d_{13}, and d_{23} values and calculated layer−layer percentage relaxations with respect to d_{bulk} values for each metal at each condition. Overall, the 0 K results generated with both RPBE and B97M-rV show acceptable expansion trends for Pt(111) and Au(111) metals, but yielding poor agreement for surface relaxations for both Cu(111) and the Ag(111) metals as shown in Figure 2 (and SI Table S1). In general, the interlayer distances for the B97M-rV functional at 0 K are more compressed with respect to experiment, and this result is independent of different plane wave cutoff values (SI Table S2) and different cell sizes and different numbers of frozen layers used to enforce the bulk lattice constant of the meta-GGA DFT model (SI Table S3). Overall, the strong contraction of interlayer relaxation for B97M-rV relative to RPBE at 0 K is attributable to the inclusion of the dispersion term in the DFT functional. To illustrate that it is not an isolated issue with the meta-GGA functional, we also evaluated the interlayer relaxations comparing RPBE with and without the D3 van der Waals correction,[62] and we also see a significant compaction trend at 0 K with inclusion of dispersion (SI Table S4).

To match the thermodynamic condition of the surface science experiments, the properties evaluated with DFT are collected as thermal averages of surface strain and bulk metal properties, which are also provided in Figure 2 (and SI Table S1). We note that previous experimental work has estimated a lattice heating time constant on the 1−10 ps time scale for 20 nm metal films for Cu and Au,[63] which would suggest that the 2.0 ps AIMD simulation time scales (the first 0.5 ps are discarded as equilibration) are sufficient for our simulated ∼1 nm thick metals. For the RPBE functional at 300 K, the thermal effects weaken the M···M interactions and induce more flexibility, resulting in a larger $\langle d_{bulk} \rangle$ that increases absolute error with respect to experiment (SI Table S1). Previous work has reported that RPBE severely underestimates cohesive energies of the four transition metals examined here,[64] which likely explains the uniform expansion of the $\langle d_{bulk} \rangle$ values when thermal energy is added, and for the high distortions we observed in the NVT ensemble by imposing the bulk lattice constant. The ambient temperature results for the B97M-rV functional corrects the 0 K surface relaxation percentages significantly, and trends are more consistent with the experimental data for all M(111) surfaces. This is especially true for the Ag(111) surface at 300 K, in which only the B97M-rV functional correctly predicts the greater contraction for $\langle d_{12} \rangle$ and more expansion for $\langle d_{23} \rangle$, in good agreement with experimental observations. For both the GGA and meta-GGA functionals, the fluctuations of the interlayer distances $\langle d_{13} \rangle$ and $\langle 2d_{bulk} \rangle$ are generally anticorrelated (SI Figure S2) to maintain the stability of the whole surface. The improvement to the $\langle d_{13} \rangle$ relaxation for B97M-rV especially is attributable to its convergence to the same average $\langle 2d_{bulk} \rangle$ value not seen at 0 K (SI Table S1).

Metal Surfaces with CO Adsorbates

Experimental adsorption enthalpies and CO site preferences at finite temperature for Cu(111) occurs in the order *atop* > *fcc* > *hcp* > *bridge*,[49,65] whereas experimental adsorption enthalpies for all other M(111) metals report only the *atop* site binding energy, as that site is thought to be strongly preferred with respect to the multicoordinated sites.[20,47,66] Figure 3 contains the DFT results using the RPBE and B97M-rV functionals for CO binding energy at 0 K at 25% coverage for the more strongly binding Cu(111) and Pt(111) metal surfaces; numerical results are also reported in SI Table S5 along with available adsorption energies generated for RPA at 0 K for comparison.[24]

https://doi.org/10.1021/jacsau.1c00300
JACS Au XXXX, XXX, XXX−XXX

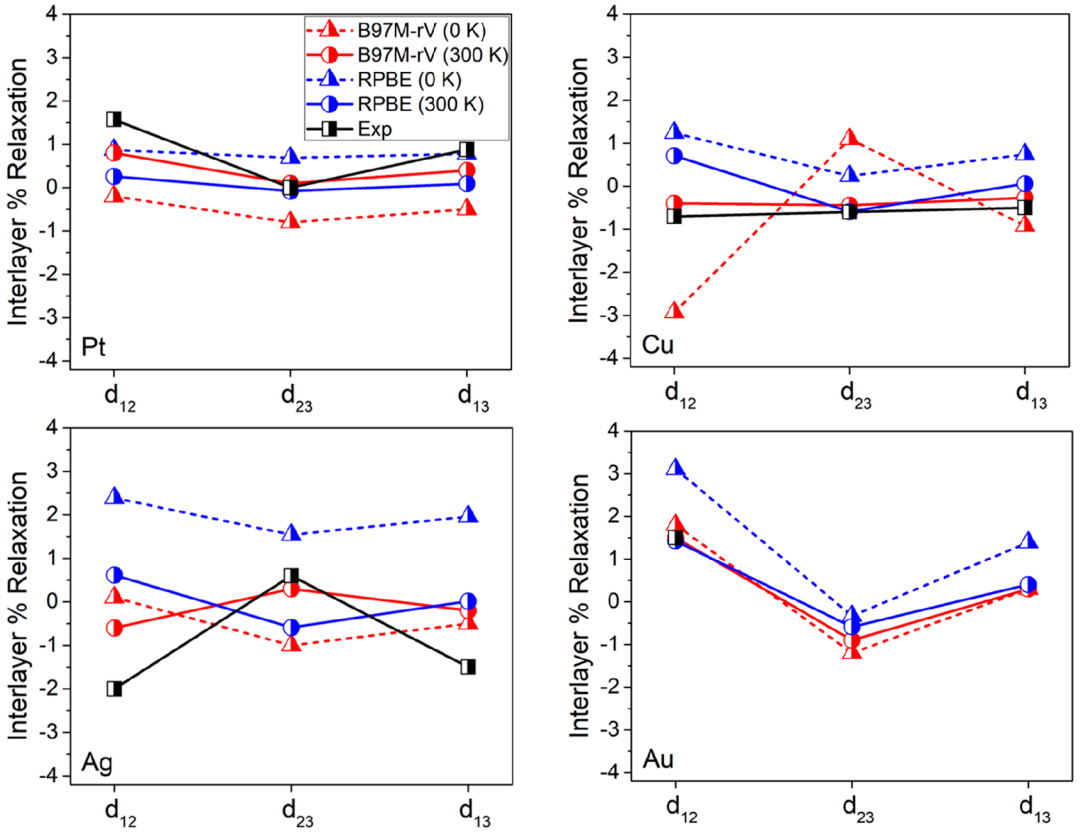

Figure 2. Calculated interlayer relaxation (%) of M(111) (M = Pt, Cu, Ag, Au) surfaces. Experimental results are also depicted here for comparison. The absent error bars are all less than 0.07 Å, relative to the DFT functional dependent layer−layer distances in the bulk. d_{12}, d_{23}, and d_{13} correspond to d_{12}/d_{bulk}, d_{23}/d_{bulk}, and $d_{13}/2d_{bulk}$, respectively, consistent with SI Table S1. Legend in Pt subfigure also applies to the other metal surfaces. Experimental data shown is for Pt(111),[56−58] Cu(111),[58,59] Ag(111),[58,60] and Au(111).[58,61]

As previously stated, at 0 K, the lower rung functionals overbind the CO on the two metals and are inconsistent in their prediction of the preferred adsorption site, whereas the RPA functional is in very good agreement with experiment for both quantities. In particular, it is known that RPA significantly modifies the metal *n*d states and CO 5σ and 2π* frontier orbitals, which is believed to determine the adsorption site preference[24] and diminishes the overbinding problem of lower rung functionals for these strong binding metals.[26] Previous work for CO on Cu found that time scales for phonon coupling is on the ∼1 ps time scale,[67] and therefore, our AIMD simulation time scales are sufficient for establishing at least CO enthalpy binding trends on all metals examined here. Figure 3 displays the DFT results using the RPBE and B97M-rV functionals for CO binding stability at 25% coverage at 300 K for the more strongly binding Pt(111) and intermediate-binding Cu(111) metal surfaces; numerical results are also reported in SI Table S5.

We find that both DFT functionals at 300 K improve their agreement with experiment for the CO chemisorption enthalpies on Cu(111), such that thermalization corrects the overbinding at 0 K (Figure 3a and b, Table S5), and both functionals prefer the *atop* site for CO binding to Cu(111) at 300 K. On the basis of the calculated $g_{M\text{-}C}(r)$ radial distribution function, integration under the first peak indicates that there is 100% chemisorbed CO at any temperature for both DFT functionals on both surfaces (SI Figure S3) with 25% CO coverage. We find that thermal fluctuations create longer M−C distances as the main indicator of a weakened bonding interaction between the metal at the *atop* site and the adsorbed CO relative to 0 K (Figure 3d and SI Table S6).

However, with thermalization, the RPBE functional now slightly underbinds CO to Cu(111) on average and does not predict the experimental trends for the other sites, likely due to lack of dispersion and possibly the large core pseudopotential. By contrast the meta-GGA functional with an optimized small core pseudopotential at 300 K predicts the relative binding enthalpies, and binding energy trend with coordination site, correctly. In fact, B97M-rV correctly ranks the *bridge* site as least stable for CO on Cu(111) as is evident from the dynamics which show significant lateral movement on the metal surface (Figure 3c). For Pt(111), the CO binding enthalpy at the *atop* site of the metal is strongly preferred with the RPA functional and is in good numerical agreement with experiment (Table S5), while for the RPBE functional there is a stronger preference for the CO to bind at the *hcp* site at 0 and 300 K. Although CO on Pt(111) is still overbound by ∼0.3 eV/CO using B97M-rV at 300 K, it also prefers the *atop* site in agreement with RPA and experiment. And we observe no lateral movements on the Pt(111) surface on the AIMD time scale.

The same calculations were performed for CO adsorption on the *atop* site of the Ag(111) and Au(111) metal surfaces (Figure 4). For the RPBE functional at either temperature, CO is predicted to be more stable in the gas phase for the two weaker binding metal surfaces, given their positive adsorption energies (SI Table S5). The first $g_{M\text{-}C}(r)$ peak gradually shrinks in the simulations over time, indicating that the number of initially bound CO molecules on Au(111) and Ag(111) surfaces is

https://doi.org/10.1021/jacsau.1c00300
JACS Au XXXX, XXX, XXX−XXX

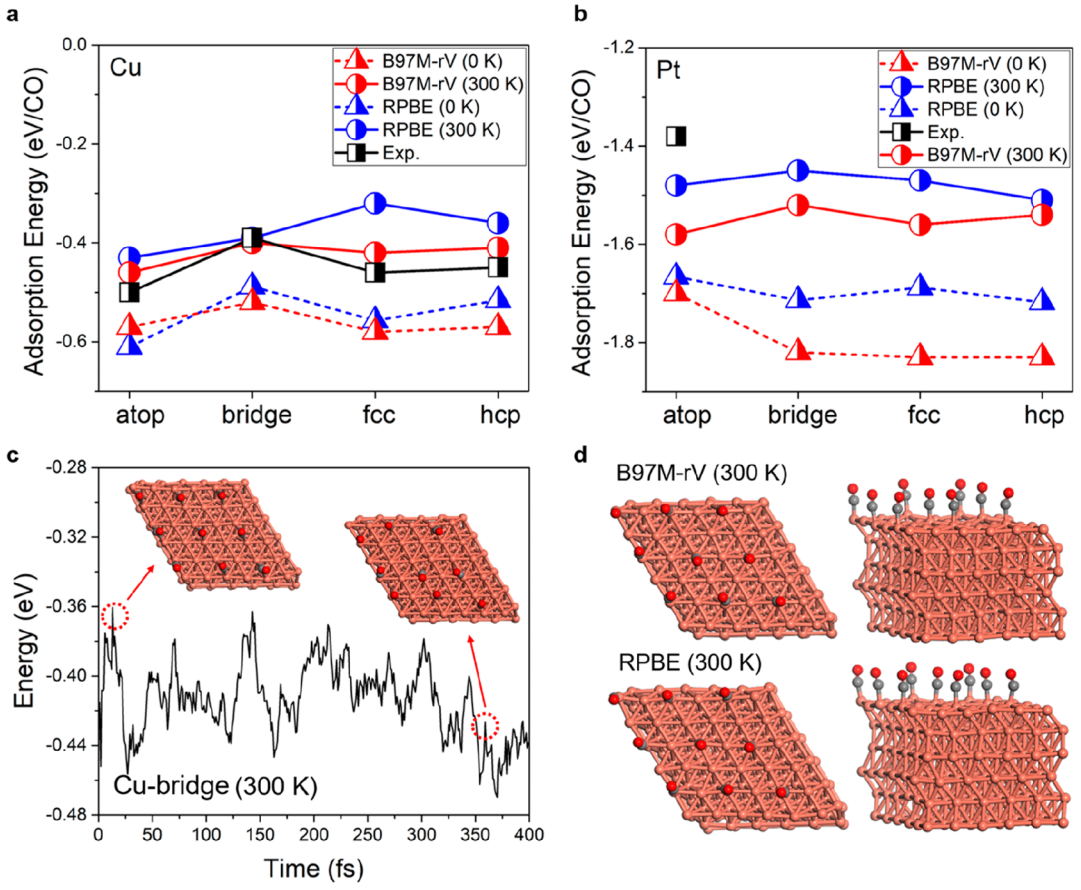

Figure 3. Thermal effects on the adsorption energies for 25% CO coverage on Cu(111) and Pt(111) surfaces. Calculated and experimentally observed adsorption enthalpies for CO on the *atop*, *bridge*, *fcc*, and *hcp* sites at 0 and 300 K for (a) Cu(111) and (b) Pt(111) (see SI Table S5 for numerical values). (c) Adsorption energy vs time for B97M-rV, illustrating CO adsorbed on Cu(111) surface at the bridge site for the first 400 fs at 300 K, but moving to the *atop* position due to the strong energetic preference for CO binding at this site. (d) Representative geometries from two different perspectives of the CO adsorbed on Cu(111) at the *atop* site for both B97M-rV and RPBE, showing the deviations from linearity of the M−C═O angle at 300 K. Absent error bars for the calculations among 15 independent trajectories are all less than 0.03 eV/CO. Experiments for CO on Pt(111) and Cu(111) are reported in refs 10, 20, 46−52, and 65. Throughout the cited literature, E_a is a constant over a wide range of temperatures, and the $\Delta H_{ads} = E_a + RT$.

decreasing. We observe the near complete dissociation of the nine COs from Ag(111) on the 2 ps time scale of the AIMD simulation for RPBE. The observation that CO effectively does not bind to the weak metal surfaces using the RPBE functional, with or without thermalization, arises in part from the lack of dispersion,[21] unlike the B97M-rV functional.

To validate the effect of dispersion for the binding behavior, we carried out RPBE-D3 calculations (SI Table S7) which predict a nontrivial adsorption on these two weak surfaces Ag(111) and Au(111), but now revealing a strong overbinding of CO on Pt(111) and Cu(111) surfaces. Similar conclusions with regard to dispersion corrections was also investigated by Grimme on various closely related surface−adsorbate systems.[68] In fact B97M-rV exhibits binding enthalpies that agree with experiment on the *atop* site for both metals and both 0 and 300 K. More interestingly, the thermalized weak binding surfaces reveal a mixture of chemisorbed/physisorbed CO molecules for the meta-GGA functional, with approximately four CO (∼44%) and approximately five CO (∼56%) molecules chemisorbed on the Ag(111) and Au(111) surfaces, respectively, with the remaining COs located up to ∼4.0 Å from the adsorption site as the evidence for physisorption. Thermal fluctuations drive toward much smaller M−C−O angles and longer M−C distances for the chemisorbed species at the *atop* site on the Au(111) and Ag(111) surfaces and thus would diminish the binding strength further compared to the stronger binding Pt(111) and Cu(111) metals (SI Table S6).

DISCUSSION

It may be asked whether free energy and/or zero point energy (ZPE) corrections should be used[69−73] for the surface adsorption of CO on the M(111) surfaces investigated here. Since the surface science experiments are in fact reporting enthalpies of CO binding on M(111) at the different sites, the correct comparison is to evaluate enthalpies of binding only. However, it raises a subtle point that the free energy determines adsorbate site preferences and thus will be relevant for microkinetic models.[19,66,71,74]

Guo et al.[43] achieved a very important advancement by performing umbrella-sampling molecular dynamics to determine the free energies of CO adsorption/desorption using the PBE functional to solve "the CO puzzle" for Pt(111),[23,75] i.e., the prediction of the correct binding site preference. The 1D reaction coordinate used by Guo and co-workers, the distance between the metal of the adsorbate site relative to center of mass of CO, is largely equivalent to the lattice gas-harmonic oscillator (LGHO) model.[43] This is shown by the fact that this same correction used on the 0 K surface for CO on the atop site of

https://doi.org/10.1021/jacsau.1c00300
JACS Au XXXX, XXX, XXX−XXX

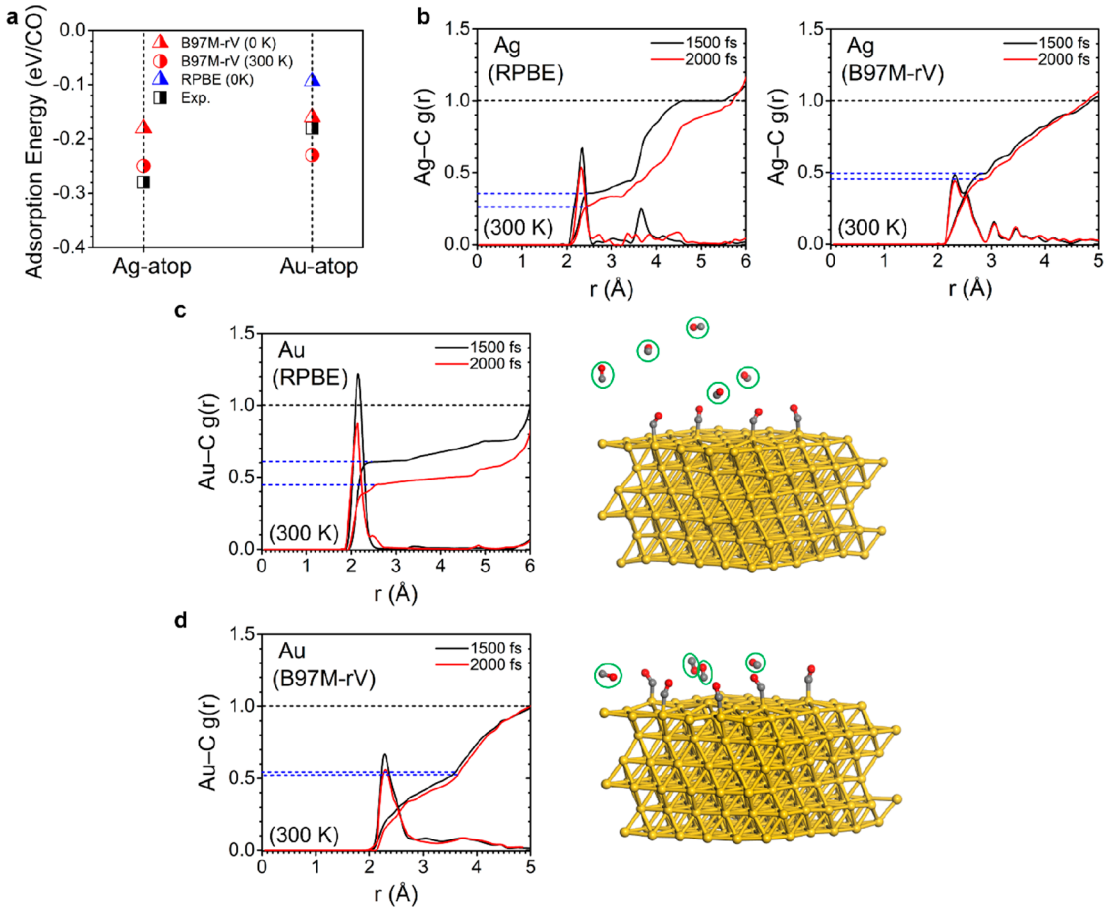

Figure 4. Thermal effects on the adsorption energies for 25% CO coverage on Ag(111) and Au(111) surfaces. (a) Calculated and experimentally observed chemisorption energies for CO on the *atop* site at 0 and 300 K for RPBE and B97M-rV. Experimental energies for CO binding: for Ag(111)[53] and for Au(111) as an average over two reported values.[17,18] (b) Radial distribution function (RDF) between the Ag metal and carbon of CO, $g_{Ag-C}(r)$, for RPBE and B97M-rV after 1.5 ps (black) and 2.0 ps (red) at 300 K, and the corresponding integration to assess the running coordination number across the 9 *atop* sites on the surface. The blue dashed lines correspond to the chemical adsorption, and the region between blue and black dashed lines represents the physical adsorption; beyond this, the RDFs are probing second nearest neighbors. (c) RPBE and (d) B97M-rV results at 300 K for Au(111) showing $g_{Au-C}(r)$ and representative snapshots showing the mixture of chemisorbed, physisorbed, and/or desorbed CO molecules (circled in green) at the last 2.0 ps time point of the AIMD simulation. The statistical data is collected after 500 fs pre-equilibration for the 2 ps trajectories. Experimental numbers for Ag(111) are taken from McElhiney and co-workers.[53] Experimental numbers for Au(111) are taken from the TPD studies of Engelhart et al.[18]

Pt(111) gave nearly an identical free energy value as the 1D umbrella sampling calculation at 300 K.[43] The LGHO model also did not correctly differentiate among the competing binding sites for CO, whereas the free energy calculation found that the multicoordinated sites become more unstable by ∼0.06 eV relative to the *atop* site.

We have performed an LGHO correction for CO binding on Pt(111) (including ZPE corrections) using the RPBE functional at 0 K and find that such a calculation also prefers the multicoordinated sites relative to the *atop* site (SI Figure S3a). Sprowl and co-workers have shown that the LGHO model breaks down when kT is less than the barriers to the in-plane translational and rotational diffusion, while for high temperatures and/or low barriers a 2D free translation/rotation (2DFree) model might be preferred instead.[71] Using a 2DFree model, we find that CO still prefers the multicoordinated sites relative to the atop site for Pt(111) (SI Figure S3b). Energy corrections for CO binding on Pt(111) surface at the *atop* and *hcp* sites from all approximations are shown in SI Figure S4, including enthalpies and free energies. Our ensemble-averaged enthalpies (ΔH, 300 K) successfully predict the *atop* site with respect to *hcp* site but still overestimate the binding by ∼0.2 eV/CO compared with experimental observation. Other models such as the harmonic LGHO and 2DFree methods fail to unravel the site preference because of the lack consideration of surface relaxations.

Additional thermodynamic issues arise when considering the Au(111) and Ag(111) metals for which the LGHO and 2DFree corrections, or a 1D reaction coordinate in conventional umbrella sampling, will certainly fail because of the low barriers to translation and rotation in all directions, and thus, the entropic difference between the unbound and bound states becomes much less significant. Even for Cu(111), we found that our unconstrained simulation shows lateral surface movement from the *bridge* to *atop* site, correctly treating the full dimensional diffusion space to determine the correct site preferences (Figure 3c).

We believe a few additional general trends learned in this work on RPBE and B97M-rV in particular will hold when evaluating any DFT functional. Thermal effects are seen to populate different normal modes of the metal surface, causing a significant change in their surface relaxation profiles. Because these surface

https://doi.org/10.1021/jacsau.1c00300
JACS Au XXXX, XXX, XXX−XXX

strain trends correlate with CO binding motifs, thermalized statistical averaging influences the preferred CO adsorption site and the relative strength of binding to other sites on any given metal surface. Although predicting the CO absorption preference on the *atop* site of electrocatalytic metals has eluded most DFT functionals previously, we expect that DFT functionals which are more accurate for intermolecular interactions, when properly evaluated at ambient conditions, will on average perform better for justifiable reasons. In this work, we have found that the B97M-rV functional determines the correct *atop* site preference for all four M(111) surfaces using an enthalpy calculation evaluated consistently with experiment, whose origin we attribute to the surface relaxation of the metal itself.

CONCLUSIONS

In this work, we have compared two different DFT functionals, the GGA RPBE and the meta-GGA B97M-rV, which were chosen for several reasons. First and foremost, they are computationally affordable when one looks ahead to the next goal of atomistic modeling of the solid−liquid interface. Second the RPBE functional[21] has become a popular choice for surface science studies and electrocatalysis applications,[64] whereas meta-GGAs such as the B97M-rV functional[40,41,76] are still undergoing evaluation across a range of applications.[39,42,77,78] Finally, we believe that several general conclusions can be drawn about DFT performance in regards the thermodynamic evaluations we have performed for these two functionals specifically.

Previous work has reported that the overall performance of RPBE for lattice parameters, cohesive energies, and surface energies of the four transition metals examined here is worse than that of the parent PBE functional,[64] in spite of its better performance for describing chemisorption energies for molecules like CO. This would suggest that RPBE at 0 K has a reliance on the severe underestimation of cohesive metal energies[64] to create reasonable metal configurations to enable good CO binding trends across a range of metals. But we find that all of the metals systematically expand when RPBE is simulated at 300 K, which is manifest in both underbinding and inconsistent site preferences for CO binding on Cu(111) and Pt(111), and complete CO desorption on the Ag(111) and Au(111) surfaces (even given the short length of our AIMD simulations), a result consistent with its lack of any dispersion model.

The metal surface contractions evaluated with the B97M-rV functional evaluated at 0 K are greater than RPBE and experiment, and thus, thermal energy systematically expands the metal surfaces too, but now in such a way to describe more correctly all interlayer distances and surface relaxation properties of the four metals. Consistent with these findings, the B97M-rV functional at 300 K systematically prefers the *atop* adsorption site for CO for the Cu(111) and Pt(111) surfaces and reproduces the relative binding energy trends for the remaining multicoordinated sites for Cu(111), and CO is found to weakly bind to the *atop* adsorption site for Ag(111) and Au(111) surfaces with energetics in excellent agreement with the experimental observations. Although the AIMD simulations used here are not as long as we would like, we expect the following qualitative results to hold with B97M-rV, namely, that while the Pt(111) and Cu(111) surfaces show complete chemisorption of CO the experiments may actually be reporting an average of chemisorbed and a small fraction of physisorbed species on the Ag(111) and Au(111) surfaces. Furthermore, because the B97M-rV meta-GGA gives an excellent description of bulk water properties,[40,41,76] combined with this work it better establishes a theoretical foundation for describing the electrolyte properties at the electrocatalytic surface in the future.[7]

In summary, the continued quest to find reliable theory to understand electrocatalytic mechanisms has traditionally focused on better quantum mechanics but less so on the statistical mechanics that is often required to match the laboratory conditions. In this work, we have shown that separation of these theoretical frameworks ignores the true nature of statistical fluctuations on top of what may or may not be a reasonable potential energy surface with a given level of quantum mechanics. That is, the relative performance of any DFT functional at 0 K for describing interlayer relaxations and CO adsorption energies at 300 K is not always reliable, and a more meaningful comparison is the ability to describe an experiment at or near the thermodynamic state point at which enthalpy data is collected.

At the same time, we certainly have not resolved all key questions and issues around electrocatalysis modeling. These issues include overcoming the self-interaction errors of non-hybrid functionals with higher rung functionals,[79] improving the quality of pseudopotentials and basis sets for new functionals[42] which we have recently accomplished for B97M-rV and ωB97M-V,[54] accounting for zero point energy,[10] electronic-vibrational coupling,[14−16] and spin−orbit relativistic effects,[68] and reducing the underappreciated differences in software packages and software settings (basis sets, distance cutoffs, numerical quadrature). Nonetheless, our results suggest that even lower-rung DFT functionals might be better than we thought for surface science and electrocatalysis, or at least not as bad as we feared, upon full consideration of the detailed fluctuations of a complete statistical mechanical ensemble.

MATERIALS AND METHODS

All calculations were carried out with DFT using the dispersion corrected meta-GGA functional B97M-rV[40,41] and revised GGA RPBE[21] in combination with TZVP basis sets optimized for multigrid integration[80] as implemented in the CP2K package.[81] The norm-conserving pseudopotentials[82] were used for describing the interactions between the frozen cores and electrons in valence shells. The development and performance of the optimized B97M-V pseudopotentials and corresponding basis sets are reported in our recent publication.[54] In all cases, we used periodic boundary conditions with a cutoff value of 400 Ry and relative cutoff of 60 Ry. All the slabs were repeated periodically with a 30 Å vacuum layer between the images in the direction of the surface normal.

Static 0 K Calculations

In the GPW formalism, the same level of accuracy can be obtained with either supercells or a k-point mesh. Based on previous work, we established a bulk model within the GPW formalism, by replicating the unit cell four times along the three cell axes to create a supercell (gamma point sampling).[42] Using the parameters obtained from bulk calculations, the slab model was built with a different number of surface layers for testing. Results presented in the main text at 0 K are for the case of a $6 \times 6 \times 6$ supercell with the three bottom layers frozen. For the CO adsorbed systems at a coverage of ∼0.25, nine CO molecules were put onto the surface at equal spacing. During the geometry optimizations, the converged criteria were 3×10^{-3} bohr for atomic displacements and 4.5×10^{-4} hartree/bohr for the forces.

AIMD Simulations at 300 K

All *ab initio* molecular dynamics simulations with the B97M-rV functional were performed by sampling in the canonical (NVT)

https://doi.org/10.1021/jacsau.1c00300
JACS Au XXXX, XXX, XXX−XXX

ensemble at 300 K employing default parameters of the canonical sampling through velocity rescaling (CSVR) algorithm implemented in CP2K,[83] with a slab model for all M(111) systems containing $6 \times 6 \times 6$ atoms for which no layers were fixed, with a time step of 1 fs (SI Figure S5). The same NVT protocol was used for the RPBE functional for Pt(111) and Cu(111), but the NVT simulations led to large distortions of the structure for Ag(111) and Au(111) metals; the RPBE metal slab model was improved by using the isobaric−isothermal ensemble (NPT) ensemble at atmospheric pressure for these metals and optimized to a stable structure but not to the experimental one. Statistical averages were collected over 2 ps of production after 0.5 ps equilibration, for which convergence was measured by the settling of the energy fluctuations to ∼0.25 kcal mol^{-1} per atom. We used the equilibrated structure and added CO adsorbates onto different sites of the surface according to the geometries obtained in the static calculations and then ran an additional 1.5 ps starting from 15 independent equilibrated trajectories of the surface calculations, important for the multicoordinated sites to address the issue of delocalized chemisorption states.[43] The time-averaged distances and adsorption energies are generated from all the trajectories during equilibration. Herein, the time-averaged adsorption energy is calculated as

$$\langle \Delta E_{ads} \rangle_{300K} = [\langle E(\mathrm{M{-}9CO}) \rangle_{300K} - 9\langle E(\mathrm{CO}) \rangle_{300K} - \langle E(\mathrm{M}) \rangle_{300K}]/9$$

To quantify the error of the statistical values, we consider the standard deviation based on the distance and energy fluctuations:

$$\sigma = \sqrt{\frac{1}{N}\sum_{i}^{N} (X_i - \langle X_i \rangle)^2}$$

The time-averaged $\overline{X_i}$ value is collected at each 100 fs time point.

■ ASSOCIATED CONTENT

Supporting Information

The Supporting Information is available free of charge at https://pubs.acs.org/doi/10.1021/jacsau.1c00300.

Interlayer surface relaxations for all M(111) using RPBE and B97M-rV; interlayer distances of Pt(111) surface using B97M-rV with different cutoff, relative cutoff values, cell sizes, and number of frozen layers; tabulated simulated and experimental adsorption energies for CO on different sites of M(111) using RPBE, RPBE with D3; B97M-rV; geometric parameters for CO adsorption on *atop* sites of M(111) surfaces; adsorption free energy corrected by various free energy approximations for Pt(111) surface for RPBE and B97M-rV; radial distribution functions $g_{M-C}(r)$ and the corresponding integration to determine coordination (PDF)

■ AUTHOR INFORMATION

Corresponding Author

Teresa Head-Gordon − *Chemical Sciences Division, Lawrence Berkeley National Laboratory, Berkeley, California 94720, United States; Kenneth S. Pitzer Center for Theoretical Chemistry, University of California, Berkeley, California 94720, United States; Department of Chemistry, Department of Chemical and Biomolecular Engineering, and Department of Bioengineering, University of California, Berkeley, California 94720, United States;* orcid.org/0000-0003-0025-8987; Email: thg@berkeley.edu

Authors

Wan-Lu Li − *Chemical Sciences Division, Lawrence Berkeley National Laboratory, Berkeley, California 94720, United States; Kenneth S. Pitzer Center for Theoretical Chemistry, University of California, Berkeley, California 94720, United States; Department of Chemistry, University of California, Berkeley, California 94720, United States*

Christianna N. Lininger − *Chemical Sciences Division, Lawrence Berkeley National Laboratory, Berkeley, California 94720, United States; Kenneth S. Pitzer Center for Theoretical Chemistry, University of California, Berkeley, California 94720, United States; Department of Chemical and Biomolecular Engineering, University of California, Berkeley, California 94720, United States*

Kaixuan Chen − *Chemical Sciences Division, Lawrence Berkeley National Laboratory, Berkeley, California 94720, United States; Kenneth S. Pitzer Center for Theoretical Chemistry, University of California, Berkeley, California 94720, United States; Department of Chemistry, University of California, Berkeley, California 94720, United States;* orcid.org/0000-0002-7864-7440

Valerie Vaissier Welborn − *Chemical Sciences Division, Lawrence Berkeley National Laboratory, Berkeley, California 94720, United States; Kenneth S. Pitzer Center for Theoretical Chemistry, University of California, Berkeley, California 94720, United States; Department of Chemistry, University of California, Berkeley, California 94720, United States; Department of Chemistry, Virginia Tech, Blacksburg, Virginia 26067, United States;* orcid.org/0000-0003-0834-4441

Elliot Rossomme − *Kenneth S. Pitzer Center for Theoretical Chemistry, University of California, Berkeley, California 94720, United States; Department of Chemistry, University of California, Berkeley, California 94720, United States*

Alexis T. Bell − *Chemical Sciences Division, Lawrence Berkeley National Laboratory, Berkeley, California 94720, United States; Department of Chemical and Biomolecular Engineering, University of California, Berkeley, California 94720, United States;* orcid.org/0000-0002-5738-4645

Martin Head-Gordon − *Chemical Sciences Division, Lawrence Berkeley National Laboratory, Berkeley, California 94720, United States; Kenneth S. Pitzer Center for Theoretical Chemistry, University of California, Berkeley, California 94720, United States; Department of Chemistry, University of California, Berkeley, California 94720, United States;* orcid.org/0000-0002-4309-6669

Complete contact information is available at: https://pubs.acs.org/10.1021/jacsau.1c00300

Author Contributions

W.-L.L. and T.H.-G. designed research; W.-L.L. and C.L. performed calculations; W.-L.L. and T.H.-G. analyzed data and data trends; W.-L.L. and T.H.-G. wrote the paper; W.-L.L. created figures; and all authors contributed discussion and insights and provided editorial comments on the paper.

Notes

The authors declare no competing financial interest.

■ ACKNOWLEDGMENTS

This work received partial support by the U.S. Department of Energy, Office of Science, Office of Advanced Scientific Computing Research, Scientific Discovery through Advanced Computing (SciDAC) program for methods development. This work was partially supported under the CPIMS program by the Director, Office of Science, Office of Basic Energy Sciences, Chemical Sciences Division of the U.S. Department of Energy

under Contract No. DE-AC02-05CH11231 for the application area of gas−solid interfaces. This work used the resources of the National Energy Research Scientific Computing Center, a DOE Office of Science User Facility supported by the Office of Science of the U.S. Department of Energy under Contract No. DE-AC02-05CH11231.

REFERENCES

(1) Hoshi, N.; Kato, M.; Hori, Y. Electrochemical reduction of CO2 on single crystal electrodes of silver Ag(111), Ag(100) and Ag(110). *J. Electroanal. Chem.* **1997**, *440* (1), 283−286.
(2) Durand, W. J.; Peterson, A. A.; Studt, F.; Abild-Pedersen, F.; Nørskov, J. K. Structure effects on the energetics of the electrochemical reduction of CO2 by copper surfaces. *Surf. Sci.* **2011**, *605* (15), 1354−1359.
(3) Lu, Q.; Rosen, J.; Zhou, Y.; Hutchings, G. S.; Kimmel, Y. C.; Chen, J. G.; Jiao, F. A selective and efficient electrocatalyst for carbon dioxide reduction. *Nat. Commun.* **2014**, *5* (1), 3242.
(4) Handoko, A. D.; Wei, F.; Jenndy; Yeo, B. S.; Seh, Z. W. Understanding heterogeneous electrocatalytic carbon dioxide reduction through operando techniques. *Nature Catalysis* **2018**, *1* (12), 922−934.
(5) Bell, A. T.; Head-Gordon, M. Quantum Mechanical Modeling of Catalytic Processes. *Annu. Rev. Chem. Biomol. Eng.* **2011**, *2*, 453−477.
(6) Abidi, N.; Lim, K. R. G.; Seh, Z. W.; Steinmann, S. N. Atomistic modeling of electrocatalysis: Are we there yet? *Wiley Interdiscip. Rev.: Comput. Mol. Sci.* **2021**, *11* (3), e1499.
(7) Seh, Z. W.; Kibsgaard, J.; Dickens, C. F.; Chorkendorff, I.; Nørskov, J. K.; Jaramillo, T. F. Combining theory and experiment in electrocatalysis: Insights into materials design. *Science* **2017**, *355* (6321), eaad4998.
(8) Cohen, A. J.; Mori-Sánchez, P.; Yang, W. Challenges for Density Functional Theory. *Chem. Rev.* **2012**, *112* (1), 289−320.
(9) Vydrov, O. A.; Van Voorhis, T. Nonlocal van der Waals Density Functional Made Simple. *Phys. Rev. Lett.* **2009**, *103* (6), 063004.
(10) Abild-Pedersen, F.; Andersson, M. P. CO adsorption energies on metals with correction for high coordination adsorption sites − A density functional study. *Surf. Sci.* **2007**, *601* (7), 1747−1753.
(11) Garrity, K. F.; Bennett, J. W.; Rabe, K. M.; Vanderbilt, D. Pseudopotentials for high-throughput DFT calculations. *Comput. Mater. Sci.* **2014**, *81*, 446−452.
(12) Duan, S.; Zhang, I. Y.; Xie, Z.; Xu, X. Identification of Water Hexamer on Cu(111) Surfaces. *J. Am. Chem. Soc.* **2020**, *142* (15), 6902−6906.
(13) Carrasco, J.; Hodgson, A.; Michaelides, A. A molecular perspective of water at metal interfaces. *Nat. Mater.* **2012**, *11* (8), 667−674.
(14) Tully, J. C. Dynamics of gas-surface interactions: Thermal desorption of Ar and Xe from platinum. *Surf. Sci.* **1981**, *111* (3), 461−478.
(15) Head-Gordon, M.; Tully, J. C. Molecular dynamics with electronic frictions. *J. Chem. Phys.* **1995**, *103* (23), 10137−10145.
(16) Subotnik, J. E.; Jain, A.; Landry, B.; Petit, A.; Ouyang, W.; Bellonzi, N. Understanding the Surface Hopping View of Electronic Transitions and Decoherence. *Annu. Rev. Phys. Chem.* **2016**, *67* (1), 387−417.
(17) Elliott, G. S.; Miller, D. R. In *14th Intternational Symposium on Rarefied Gas Dynamics*; University of Tokyo Press: Tokyo, 1984; pp 349−358.
(18) Engelhart, D. P.; Wagner, R. J. V.; Meling, A.; Wodtke, A. M.; Schäfer, T. Temperature programmed desorption of weakly bound adsorbates on Au(111). *Surf. Sci.* **2016**, *650*, 11−16.
(19) Campbell, C. T.; Sellers, J. R. V. Enthalpies and Entropies of Adsorption on Well-Defined Oxide Surfaces: Experimental Measurements. *Chem. Rev.* **2013**, *113* (6), 4106−4135.
(20) Wellendorff, J.; Silbaugh, T. L.; Garcia-Pintos, D.; Nørskov, J. K.; Bligaard, T.; Studt, F.; Campbell, C. T. A benchmark database for adsorption bond energies to transition metal surfaces and comparison to selected DFT functionals. *Surf. Sci.* **2015**, *640*, 36−44.
(21) Hammer, B.; Hansen, L. B.; Nørskov, J. K. Improved adsorption energetics within density-functional theory using revised Perdew-Burke-Ernzerhof functionals. *Phys. Rev. B: Condens. Matter Mater. Phys.* **1999**, *59* (11), 7413−7421.
(22) Lynch, M.; Hu, P. A density functional theory study of CO and atomic oxygen chemisorption on Pt(111). *Surf. Sci.* **2000**, *458* (1), 1−14.
(23) Feibelman, P. J.; Hammer, B.; Nørskov, J. K.; Wagner, F.; Scheffler, M.; Stumpf, R.; Watwe, R.; Dumesic, J. The CO/Pt(111) Puzzle. The. *J. Phys. Chem. B* **2001**, *105* (18), 4018−4025.
(24) Schimka, L.; Harl, J.; Stroppa, A.; Grüneis, A.; Marsman, M.; Mittendorfer, F.; Kresse, G. Accurate surface and adsorption energies from many-body perturbation theory. *Nat. Mater.* **2010**, *9* (9), 741−744.
(25) Chen, B. W. J.; Xu, L.; Mavrikakis, M. Computational Methods in Heterogeneous Catalysis. *Chem. Rev.* **2021**, *121* (2), 1007−1048.
(26) Gil, A.; Clotet, A.; Ricart, J. M.; Kresse, G.; García-Hernández, M.; Rösch, N.; Sautet, P. Site preference of CO chemisorbed on Pt(111) from density functional calculations. *Surf. Sci.* **2003**, *530* (1), 71−87.
(27) Stroppa, A.; Termentzidis, K.; Paier, J.; Kresse, G.; Hafner, J. CO adsorption on metal surfaces: A hybrid functional study with plane-wave basis set. *Phys. Rev. B: Condens. Matter Mater. Phys.* **2007**, *76* (19), 195440.
(28) Garrido Torres, J. A.; Ramberger, B.; Früchtl, H. A.; Schaub, R.; Kresse, G. Adsorption energies of benzene on close packed transition metal surfaces using the random phase approximation. *Physical Review Materials* **2017**, *1* (6), 060803.
(29) Rohlfing, M.; Bredow, T. Binding Energy of Adsorbates on a Noble-Metal Surface: Exchange and Correlation Effects. *Phys. Rev. Lett.* **2008**, *101* (26), 266106.
(30) Harl, J.; Kresse, G. Accurate Bulk Properties from Approximate Many-Body Techniques. *Phys. Rev. Lett.* **2009**, *103* (5), 056401.
(31) Ren, X.; Rinke, P.; Scheffler, M. Exploring the random phase approximation: Application to CO adsorbed on Cu(111). *Phys. Rev. B: Condens. Matter Mater. Phys.* **2009**, *80* (4), 045402.
(32) Becke, A. D. Density-functional thermochemistry. III. The role of exact exchange. *J. Chem. Phys.* **1993**, *98* (7), 5648−5652.
(33) Yu, H. S.; He, X.; Li, S. L.; Truhlar, D. G. MN15: A Kohn-Sham global-hybrid exchange-correlation density functional with broad accuracy for multi-reference and single-reference systems and noncovalent interactions. *CHEMICAL SCIENCE* **2016**, *7* (8), 5032−5051.
(34) Zhao, Y.; Truhlar, D. G. The M06 suite of density functionals for main group thermochemistry, thermochemical kinetics, noncovalent interactions, excited states, and transition elements: two new functionals and systematic testing of four M06-class functionals and 12 other functionals. *Theor. Chem. Acc.* **2008**, *120* (1−3), 215−241.
(35) Chai, J.-D.; Head-Gordon, M. Long-range corrected hybrid density functionals with damped atom−atom dispersion corrections. *Phys. Chem. Chem. Phys.* **2008**, *10* (44), 6615−6620.
(36) Sun, J.; Haunschild, R.; Xiao, B.; Bulik, I. W.; Scuseria, G. E.; Perdew, J. P. Semilocal and hybrid meta-generalized gradient approximations based on the understanding of the kinetic-energy-density dependence. *J. Chem. Phys.* **2013**, *138* (4), 044113−044113.
(37) Sun, J.; Remsing, R. C.; Zhang, Y.; Sun, Z.; Ruzsinszky, A.; Peng, H.; Yang, Z.; Paul, A.; Waghmare, U.; Wu, X.; Klein, M. L.; Perdew, J. P. Accurate first-principles structures and energies of diversely bonded systems from an efficient density functional. *Nat. Chem.* **2016**, *8* (9), 831−836.
(38) Sun, J.; Ruzsinszky, A.; Perdew, J. P. Strongly Constrained and Appropriately Normed Semilocal Density Functional. *Phys. Rev. Lett.* **2015**, *115* (3), 036402−036402.
(39) Garza, A. J.; Bell, A. T.; Head-Gordon, M. Nonempirical Meta-Generalized Gradient Approximations for Modeling Chemisorption at Metal Surfaces. *J. Chem. Theory Comput.* **2018**, *14* (6), 3083−3090.
(40) Mardirossian, N.; Ruiz Pestana, L.; Womack, J. C.; Skylaris, C.-K.; Head-Gordon, T.; Head-Gordon, M. Use of the rVV10 Nonlocal

https://doi.org/10.1021/jacsau.1c00300
JACS Au XXXX, XXX, XXX−XXX

Correlation Functional in the B97M-V Density Functional: Defining B97M-rV and Related Functionals. *J. Phys. Chem. Lett.* **2017**, *8* (1), 35−40.
(41) Mardirossian, N.; Head-Gordon, M. Mapping the genome of meta-generalized gradient approximation density functionals: The search for B97M-V. *J. Chem. Phys.* **2015**, *142* (7), 074111.
(42) Lininger, C. N.; Gauthier, J. A.; Li, W.-L.; Rossomme, E.; Welborn, V. V.; Lin, Z.; Head-Gordon, T.; Head-Gordon, M.; Bell, A. T. Challenges for density functional theory: calculation of CO adsorption on electrocatalytically relevant metals. *Phys. Chem. Chem. Phys.* **2021**, *23* (15), 9394−9406.
(43) Guo, C.; Wang, Z.; Wang, D.; Wang, H.-F.; Hu, P. First-Principles Determination of CO Adsorption and Desorption on Pt(111) in the Free Energy Landscape. *J. Phys. Chem. C* **2018**, *122* (37), 21478−21483.
(44) Wang, Y.; Babin, V.; Bowman, J. M.; Paesani, F. The Water Hexamer: Cage, Prism, or Both. Full Dimensional Quantum Simulations Say Both. *J. Am. Chem. Soc.* **2012**, *134* (27), 11116−11119.
(45) Car, R.; Parrinello, M. Unified Approach for Molecular Dynamics and Density-Functional Theory. *Phys. Rev. Lett.* **1985**, *55* (22), 2471−2474.
(46) Karp, E. M.; Campbell, C. T.; Studt, F.; Abild-Pedersen, F.; Nørskov, J. K. Energetics of Oxygen Adatoms, Hydroxyl Species and Water Dissociation on Pt(111). *J. Phys. Chem. C* **2012**, *116* (49), 25772−25776.
(47) Brown, W.; Kose, R.; King, D. Femtomole adsorption calorimetry on single-crystal surfaces. *Chem. Rev.* **1998**, *98* (2), 797−832.
(48) Schießer, A.; Hörtz, P.; Schäfer, R. Thermodynamics and kinetics of CO and benzene adsorption on Pt(111) studied with pulsed molecular beams and microcalorimetry. *Surf. Sci.* **2010**, *604* (23), 2098−2105.
(49) Hollins, P.; Pritchard, J. Interactions of CO molecules adsorbed on Cu(111). *Surf. Sci.* **1979**, *89* (1), 486−495.
(50) Campbell, C. T.; Ertl, G.; Kuipers, H.; Segner, J. A molecular beam study of the adsorption and desorption of oxygen from a Pt(111) surface. *Surf. Sci.* **1981**, *107* (1), 220−236.
(51) Kelemen, S. R.; Fischer, T. E.; Schwarz, J. A. The binding energy of CO on clean and sulfur covered platinum surfaces. *Surf. Sci.* **1979**, *81* (2), 440−450.
(52) Poelsema, B.; Palmer, R. L.; Comsa, G. A thermal He scattering study of CO adsorption on Pt(111). *Surf. Sci.* **1984**, *136* (1), 1−14.
(53) McElhiney, G.; Papp, H.; Pritchard, J. The adsorption of Xe and CO on Ag(111). *Surf. Sci.* **1976**, *54* (3), 617−634.
(54) Li, W.-L.; Chen, K.; Rossomme, E.; Head-Gordon, M.; Head-Gordon, T. Optimized pseudopotentials and basis sets for semi-empirical Density Functional Theory for electrocatalysis applications. Submitted, **2021**.
(55) Mavrikakis, M.; Hammer, B.; Nørskov, J. K. Effect of Strain on the Reactivity of Metal Surfaces. *Phys. Rev. Lett.* **1998**, *81* (13), 2819−2822.
(56) Materer, N.; Barbieri, A.; Gardin, D.; Starke, U.; Batteas, J. D.; Van Hove, M. A.; Somorjai, G. A. Dynamical LEED analyses of the Pt(111)-p(2× 2)-NO and the Ni(111)-c(4 × 2)-2NO structures: substrate relaxation and unexpected hollow-site adsorption. *Surf. Sci.* **1994**, *303* (3), 319−332.
(57) Krupski, K.; Moors, M.; Jóźwik, P.; Kobiela, T.; Krupski, A. Structure Determination of Au on Pt(111) Surface: LEED, STM and DFT Study. *Materials* **2015**, *8* (6), 2935−2952.
(58) Wan, J.; Fan, Y. L.; Gong, D. W.; Shen, S. G.; Fan, X. Q. Surface relaxation and stress of fcc metals: Cu, Ag, Au, Ni, Pd, Pt, Al and Pb. *Modell. Simul. Mater. Sci. Eng.* **1999**, *7* (2), 189−206.
(59) Lindgren, S. Å.; Walldén, L.; Rundgren, J.; Westrin, P. Low-energy electron diffraction from Cu(111): Subthreshold effect and energy-dependent inner potential; surface relaxation and metric distances between spectra. *Phys. Rev. B: Condens. Matter Mater. Phys.* **1984**, *29* (2), 576−588.
(60) Statiris, P.; Lu, H. C.; Gustafsson, T. Temperature dependent sign reversal of the surface contraction of Ag(111). *Phys. Rev. Lett.* **1994**, *72* (22), 3574−3577.
(61) Nichols, R. J.; Nouar, T.; Lucas, C. A.; Haiss, W.; Hofer, W. A. Surface relaxation and surface stress of Au(111). *Surf. Sci.* **2002**, *513* (2), 263−271.
(62) Grimme, S.; Antony, J.; Ehrlich, S.; Krieg, H. A consistent and accurate ab initio parametrization of density functional dispersion correction (DFT-D) for the 94 elements H-Pu. *J. Chem. Phys.* **2010**, *132* (15), 154104.
(63) Ligges, M.; Rajkovic, I.; Zhou, P.; Posth, O.; Hassel, C.; Dumpich, G.; von der Linde, D. Observation of ultrafast lattice heating using time resolved electron diffraction. *Appl. Phys. Lett.* **2009**, *94* (10), 101910.
(64) Janthon, P.; Kozlov, S. M.; Viñes, F.; Limtrakul, J.; Illas, F. Establishing the Accuracy of Broadly Used Density Functionals in Describing Bulk Properties of Transition Metals. *J. Chem. Theory Comput.* **2013**, *9* (3), 1631−1640.
(65) Hinch, B. J.; Dubois, L. H. First-order corrections in modulated molecular beam desorption experiments. *Chem. Phys. Lett.* **1990**, *171* (1), 131−135.
(66) Fischer-Wolfarth, J.-H.; Hartmann, J.; Farmer, J. A.; Flores-Camacho, J. M.; Campbell, C. T.; Schauermann, S.; Freund, H.-J. An improved single crystal adsorption calorimeter for determining gas adsorption and reaction energies on complex model catalysts. *Rev. Sci. Instrum.* **2011**, *82* (2), 024102.
(67) Springer, C.; Head-Gordon, M.; Tully, J. C. Simulations of femtosecond laser-induced desorption of CO from Cu(100). *Surf. Sci.* **1994**, *320* (1), L57−L62.
(68) Grimme, S.; Hansen, A.; Ehlert, S.; Mewes, J.-M. r2SCAN-3c: A "Swiss army knife" composite electronic-structure method. *J. Chem. Phys.* **2021**, *154* (6), 064103.
(69) Wang, Z.; Liu, X.; Rooney, D. W.; Hu, P. Elucidating the mechanism and active site of the cyclohexanol dehydrogenation on copper-based catalysts: A density functional theory study. *Surf. Sci.* **2015**, *640*, 181−189.
(70) Cao, X.-M.; Burch, R.; Hardacre, C.; Hu, P. An understanding of chemoselective hydrogenation on crotonaldehyde over Pt(111) in the free energy landscape: The microkinetics study based on first-principles calculations. *Catal. Today* **2011**, *165* (1), 71−79.
(71) Sprowl, L. H.; Campbell, C. T.; Árnadóttir, L. Hindered Translator and Hindered Rotor Models for Adsorbates: Partition Functions and Entropies. *J. Phys. Chem. C* **2016**, *120* (18), 9719−9731.
(72) Motagamwala, A. H.; Dumesic, J. A. Microkinetic Modeling: A Tool for Rational Catalyst Design. *Chem. Rev.* **2021**, *121*, 1049.
(73) Grabow, L. C.; Gokhale, A. A.; Evans, S. T.; Dumesic, J. A.; Mavrikakis, M. Mechanism of the Water Gas Shift Reaction on Pt: First Principles, Experiments, and Microkinetic Modeling. *J. Phys. Chem. C* **2008**, *112* (12), 4608−4617.
(74) Jørgensen, M.; Grönbeck, H. Adsorbate Entropies with Complete Potential Energy Sampling in Microkinetic Modeling. *J. Phys. Chem. C* **2017**, *121* (13), 7199−7207.
(75) Blackman, G. S.; Xu, M. L.; Ogletree, D. F.; Van Hove, M. A.; Somorjai, G. A. Mix of Molecular Adsorption Sites Detected for Disordered CO on Pt(111) by Diffuse Low-Energy Electron Diffraction. *Phys. Rev. Lett.* **1988**, *61* (20), 2352−2355.
(76) Ruiz Pestana, L.; Mardirossian, N.; Head-Gordon, M.; Head-Gordon, T. Ab initio molecular dynamics simulations of liquid water using high quality meta-GGA functionals. *Chemical Science* **2017**, *8* (5), 3554−3565.
(77) Welborn, V. V.; Li, W.-L.; Head-Gordon, T. Interplay of water and a supramolecular capsule for catalysis of reductive elimination reaction from gold. *Nat. Commun.* **2020**, *11* (1), 415.
(78) Rossomme, E.; Lininger, C. N.; Bell, A. T.; Head-Gordon, T.; Head-Gordon, M. Electronic structure calculations permit identification of the driving forces behind frequency shifts in transition metal monocarbonyls. *Phys. Chem. Chem. Phys.* **2020**, *22* (2), 781−798.
(79) Patra, A.; Peng, H.; Sun, J.; Perdew, J. P. Rethinking CO adsorption on transition-metal surfaces: Effect of density-driven self-

https://doi.org/10.1021/jacsau.1c00300
JACS Au XXXX, XXX, XXX−XXX

interaction errors. *Phys. Rev. B: Condens. Matter Mater. Phys.* **2019**, *100* (3), 035442.
(80) VandeVondele, J.; Hutter, J. Gaussian basis sets for accurate calculations on molecular systems in gas and condensed phases. *J. Chem. Phys.* **2007**, *127* (11), 114105.
(81) Hutter, J.; Iannuzzi, M.; Schiffmann, F.; VandeVondele, J. cp2k: atomistic simulations of condensed matter systems. *WIREs Computational Molecular Science* **2014**, *4* (1), 15−25.
(82) Goedecker, S.; Teter, M.; Hutter, J. Separable dual-space Gaussian pseudopotentials. *Phys. Rev. B: Condens. Matter Mater. Phys.* **1996**, *54* (3), 1703−1710.
(83) Bussi, G.; Donadio, D.; Parrinello, M. Canonical sampling through velocity rescaling. *J. Chem. Phys.* **2007**, *126* (1), 014101.

https://doi.org/10.1021/jacsau.1c00300
JACS Au XXXX, XXX, XXX−XXX